

# Manufacture and Characterization of Dy<sub>2</sub>O<sub>3</sub> Nanoparticles via X-Ray Diffraction, TEM and Photoluminescence

Amir Zelati<sup>1\*</sup>, Ahmad Amirabadizadeh<sup>1</sup>, Ahmad Kompany<sup>2</sup>, Hadi Salamati<sup>3</sup> and Jeff Sonier<sup>4</sup>

<sup>1</sup>Department of Physics, University of Birjand, Iran; a\_zelati@yahoo.com, ahmadamirabadi@yahoo.com

<sup>2</sup>Department of Physics, Ferdowsi University of Mashhad, Iran; kompany@ferdowsi.um.ac.ir

<sup>3</sup>Faculty of Physics, Isfahan University of Technology, Iran; salamati@cc.iut.ac.ir

<sup>4</sup>Department of Physics, Simon Fraser University, Burnaby, BC, Canada; jsonier@sfu.ca

## Abstract

In this research, Dysprosium Oxide (Dysprosia) nanoparticles with the composition, Dy<sub>2</sub>O<sub>3</sub>, were prepared by using the combustion method. The precursor sol was obtained from Dysprosium Nitrate and Glycine was used as the fuel. The molar ratio of cation/glycine = 1.5 was used to prepare very fine powder of dysprosium oxide. The innovative aspect of this method is the preparation of Dy<sub>2</sub>O<sub>3</sub> nanoparticles without applying calcination temperature. To study the effect of the heating and annealing on the structural and optical properties of dysprosia, three different calcination temperatures, 450°, 550° and 650°C were applied on the initial product (no-calcined sample).

Transmission Electron Microscopy (TEM) and X-Ray Diffraction (XRD) were used for structural characterization and Photo Luminescence (PL) was used for studying optical properties of the samples. XRD patterns show the ideal cubic structure for all samples. The crystallite sizes were estimated from the broadening of XRD peaks, using Scherrer's formula. XRD estimated the crystallite sizes from 24 nm for no-calcined sample to 28 nm for the calcined sample at 650°C. TEM shows the sizes of the particles produced by this method ranged from 5 nm to 100 nm. The samples also exhibited room temperature PL, having a strong emission in the visible region. The band gap of the samples was measured by PL results.

**Keywords:** Dysprosium Oxide Nanoparticles, Combustion Method, XRD, TEM, PL.

## 1. Introduction

Nanomaterials or nanostructured materials are with structural features in between those of atoms/molecules and bulk materials, with at least one dimension in the range of 1 to 100 nm (1 nm=10<sup>-9</sup> m) [1]. In this size range, the particles have a high proportion of atoms located at its surface as compared to bulk materials, giving rise to unique physical and chemical properties that are totally different from their bulk counterparts [2]. The oxides of rare earth elements such as Y, Nd, Sm, Eu, Dy, and La are emerging as promising materials for a variety of applications in

many different fields of modern technology [3] such as catalysts, high efficiency phosphors, and magnetic to dielectric formulations for multilayer ceramic capacitors [4, 5]. Dysprosium Oxide or Dysprosia with the chemical composition Dy<sub>2</sub>O<sub>3</sub>, one of the rare earth oxide families, is a basic metal oxide and its properties are influenced by the preparation conditions. Dy<sub>2</sub>O<sub>3</sub> is a white, slightly hygroscopic powder and it is highly insoluble and thermally stable. Dysprosia has specialized uses in ceramics, glass, phosphors, lasers and dysprosium metal halide lamps [6].

There are different ways for the synthesis Dysprosia Nanoparticles such as homogenous precipitation and wet

\*Corresponding author:

Amir Zelati (a\_zelati@yahoo.com)

chemical methods. In this paper, combustion method for the preparation of  $Dy_2O_3$  nanoparticles is reported. Combustion Synthesis is an important powder processing technique generally used to produce complex oxide ceramics. This method is generally employed to prepare oxide materials. The process involves the exothermic reaction between an oxidizer such as metal nitrates and organic fuel, like urea ( $H_2NCONH_2$ ), carbonylhydrazide ( $CO(NHNH_2)_2$ ), or glycine ( $C_2H_5NO_2$ ). The combustion reaction is initiated in a muffle furnace or on a hot plate at temperatures of the order of  $500^\circ C$  or less. In a typical reaction, the precursor (mixture of water, metal nitrates and fuel) on heating decomposes, dehydrates and ruptures into a flame. The resultant product is a voluminous, foamy powder, which occupies the entire volume of the reaction vessel [1]. The chemical energy released from the exothermic reaction between the metal nitrates and fuel can rapidly heat the system to high temperatures without an external heat source. Nanomaterials synthesized by combustion route are generally homogeneous, contain fewer impurities, and have higher surface areas than powders prepared by conventional solid state methods. The major advantage of this method is that large scale production can be made at relatively low temperatures. This method is very flexible and promising technique as it is relatively simple, reproducible, and economically feasible. By using combustion route, for preparing  $Dy_2O_3$ , the final product obtained in a very short time. The innovative aspect of this method is preparation of  $Dy_2O_3$  nanoparticles without applying calcination temperature. Although the product of the combustion method with no calcination temperature was  $Dy_2O_3$  nanoparticles, for further study on the effect of the heating and annealing on the structural and optical properties of dysprosia, three different calcination temperatures,  $T = 450^\circ C$ ,  $T = 550^\circ C$  and  $T = 650^\circ C$  were applied on the initial product (no-calcined sample). Samples structural, morphological and optical properties are investigated via XRD, TEM and PL.

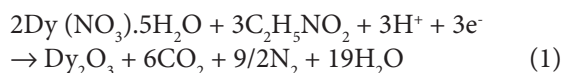
## 2. Experimental Procedure

### 2.1 Samples Preparation

In this research, combustion technique is used to prepare dysprosia nanoparticles. The ingredients used for preparing Dysprosium (III) Oxide Nanoparticles, consists of Dysprosium (III) Nitrate Pantahydrate with the chemical

formula  $Dy(NO_3)_3 \cdot 5H_2O$ , distilled water and Glycine with chemical formula  $C_2H_5NO_2$  as the fuel of the reaction. The  $Dy_2O_3$  nanopowder synthesis by the combustion method is summarized in a flow chart shown in Figure 1.

Chemical reaction formula for preparing dysprosia is shown in relation 1.



For preparing 10mL dysprosium nitrate of 3.5 N solution, 5.12 gr Dysprosium (III) Nitrate Pantahydrate was dissolved in adequate amount of distilled water. After obtaining an aqueous solution of the cation, ( $Dy^{3+}$ ), glycine as a fuel for combustion was added to the solution. This liquid mixture was stirred for 30 minutes at about  $40^\circ C$  on a hot plate. In the mean time, the furnace was heated to  $300^\circ C$ . Then the liquid mixture was placed inside the pre-heated ( $300^\circ C$ ) furnace for one hour. Combustion took place inside the furnace and russet smoke of the  $NO_2$  gas came out. The resultant product was a voluminous, foamy and white powder, which occupies the entire volume of the reaction vessel. For studying the effect of calcination temperature, the resultant powder was divided in 4 segments, One remained without calcination temperature (sample 1) and the rest were calcined at three different calcination temperatures  $T = 450^\circ C$  (sample 2),  $T = 550^\circ C$  (sample 3) and  $T = 650^\circ C$  (sample 4). Figure 2 shows the calcination diagrams of sample 2, 3 and 4. Each diagram consists of three stages. At the first stage, sample was heated to

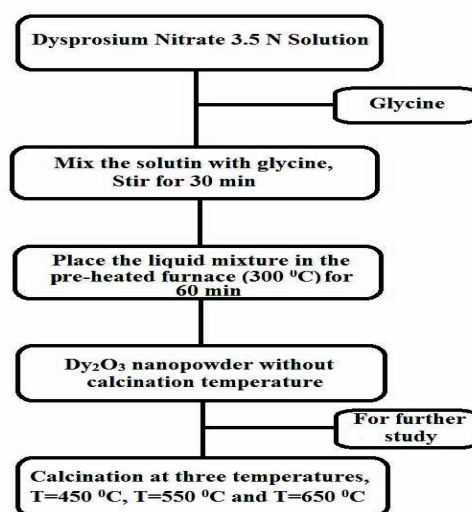


**Figure 1.** Flow chart of  $Dy_2O_3$  nanoparticles preparation by combustion process.

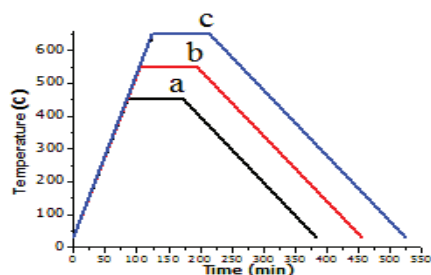


**Figure 2.** Calcination diagram of, a) sample 2, calcined at 450°C, b) sample 3, calcined at 550°C, c) sample 4, calcined at 650°C.

the calcination temperature with the ratio 5°C/min and then at the second stage, sample remained at calcination temperature for 90 minutes and at the final stage sample was cooled down to the room temperature with the ratio 2°C/min.

## 2.2 Sample Characterization

X Ray Diffraction (XRD), Transmission Electron Microscopy (TEM) and PhotoLuminescence (PL) were used for the characterization of the samples. The XRD patterns of Dy<sub>2</sub>O<sub>3</sub> nanoparticles prepared at various calcination temperatures were recorded by the D8 Advanced Bruker system using CuK $\alpha$  ( $\lambda=0.154056$  nm) radiation with  $2\theta$  in the range 10–80°. The scanning rate was 0.060°s<sup>-1</sup> in the  $2\theta$  range from 10° to 80°. The crystallite size  $d_{XRD}$  was estimated from the broadening of XRD peaks, using Scherrer's equation [7]:

$$d_{XRD} = \frac{K\lambda}{\beta \cos \theta} \quad (2)$$

where,  $\theta$  is the Bragg Angle of Diffraction Lines,

$K$  is a shape factor taken as 1,

$\lambda$  is the wavelength of incident X-rays (1.5406 Å), and  $\beta$  is the corrected Full Width at Half Maximum (FWHM) given by:

$$\beta^2 = \beta_m^2 - \beta_s^2 \quad (3)$$

where,  $\beta_m$  is the measured FWHM and  $\beta_s$  is the FWHM of a silicon standard with large crystallite size (>150 nm) that was used to determine the instrumental broadening.

TEM studies were carried out with an FEI Tecnai 20 Transmission Electron Microscope with a field-emission source operating at 200 kV. The required sample for TEM analysis was prepared by dispersing the Dy<sub>2</sub>O<sub>3</sub> nanoparticles in acetone using an ultrasound bath. A drop of this dispersed suspension was put on to 200-mesh

carbon-coated Cu grid and then was dried in vacuum [8].

The room temperature photoluminescence study was carried out using a Avaspec 2048 TEC spectrofluorometer in the range of 350–700 nm.

## 3. Results and Discussion

### 3.1 X-Ray Diffraction

The phase identification of the no-calcined and calcined powders was performed using XRD. The average crystallite size of the powders was measured by X-ray line-broadening technique employing the Scherrer's formula (2). The XRD pattern of prepared Dy<sub>2</sub>O<sub>3</sub> nanoparticles without applying calcination temperature is shown in Figure 3. It is clear that the powders, which are not calcined, are crystalline without additional phase. Because of the drastic increase of temperature in combustion process, there are strong picks of cubic structure of Dy<sub>2</sub>O<sub>3</sub>. Therefore, the innovative aspect of this method is preparation of Dy<sub>2</sub>O<sub>3</sub> nanoparticles without applying calcination temperature. To study the effect of the heating and annealing on the structural and optical properties of dysprosia, three different calcination temperatures, T=450°, 550° and 650°C were applied on the no-calcined sample. The XRD patterns of the all samples are shown in Figure 4. The Bragg's peaks of the crystallized powders correspond to each sample agree well with the reflections of pure cubic Dy<sub>2</sub>O<sub>3</sub> single phase with  $a=b=1.66500$  Å. The XRD patterns at all samples show that the intensities of 5 basic peaks of the (222), (440), (400), (622) and (211) planes are more than the other peaks [8].

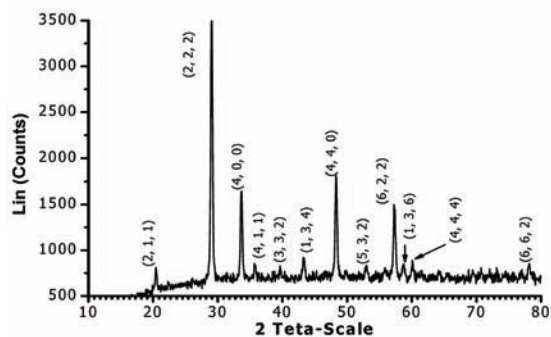


**Figure 3.** The XRD pattern of the no-calcined Dy<sub>2</sub>O<sub>3</sub> (Sample 1) nanoparticle, cubic structure, without additional phase.

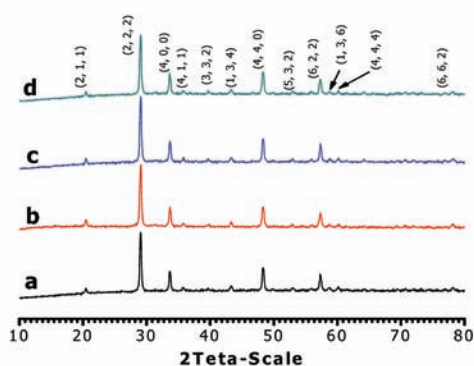


**Figure 4.** The XRD patterns of a) no-calcined sample b) calcined sample at  $T=450^{\circ}\text{C}$ , c) calcined sample at  $T= 550^{\circ}\text{C}$ , d) calcined sample at  $T=650^{\circ}\text{C}$ .

Table 1 shows the XRD parameters of  $\text{Dy}_2\text{O}_3$  nanoparticles in various crystalline orientations without calcination temperature and at different calcination temperatures. As seen in Table 1, the width of the strongest peak and most of other picks decrease with increasing of the calcination temperature, which refers to the growth of crystal size. In addition, increasing in calcination temperature leads to the more crystalline structure [8].

The crystallite size was estimated from the broadening of XRD peaks, using Scherrer's formula (2) [7]. The results of the crystallite size are shown in Table 1. As seen in Table 1 and Figure 5, the mean crystallite sizes ( $\langle d \rangle$ ) are in the nanometric orders so XRD by using Scherrer's formula (2) confirms that the samples are in nanometric sizes.

**Table 1.** The XRD parameters of nanoparticles in different crystallography orientation for no-calcined sample (sample 1) and for sample, which calcined at different calcination temperatures (Sample 1. 2 and 3).  $D$  (nm) and  $\langle d \rangle$  related to the Scherrer's formula (2)

hkl		$2\theta$ (deg)	$d(\text{\AA})$	Intensity Lin (Cps)	FWHM $2\theta$ (deg)	$D$ (nm)	$\langle d \rangle$ (nm)
Sample 1: No Calcined Sample	222	29.068	3.0705	3571	0.369	24	24
	440	48.324	1.8818	1815	0.379	23	
	400	33.671	2.6607	1646	0.355	25	
	622	57.351	1.6057	1497	0.387	23	
Sample 2: Calcined Sample at $T=450^{\circ}\text{C}$	222	29.075	3.0698	3586	0.336	26	25
	440	48.323	1.8815	1518	0.393	22.5	
	400	33.676	2.6605	1504	0.334	26.5	
	622	57.351	1.6056	1236	0.406	22	
Sample 3: Calcined Sample at $T=550^{\circ}\text{C}$	222	29.464	3.0688	3942	0.323	27.5	27
	440	48.320	1.8811	1842	0.352	25	
	400	33.683	2.6593	1754	0.323	27.5	
	622	57.351	1.6053	1607	0.337	26	
Sample 4: Calcined Sample at $T=650^{\circ}\text{C}$	222	29.062	3.0706	3969	0.321	28	28
	440	48.309	1.8823	2152	0.359	25	
	400	33.656	2.6606	1964	0.328	27	
	622	57.321	1.6056	1790	0.329	27	
	211	20.467	4.4.34	1193	0.272	32.5	

Scherrer's formula has an accurate result for single crystals while for poly crystals the result is not accurate. The advantage of the Scherrer's formula is that the nanometric order of crystallite sizes can be estimated. It is observed from Table 1, the mean crystallite sizes increase with the increasing of the calcination temperature, which refers to the more crystalline structure.

### 3.2 Transmission Electron Microscopy (TEM)

The morphology and size distribution of the no-calcined Dy<sub>2</sub>O<sub>3</sub> and Dy<sub>2</sub>O<sub>3</sub> samples calcined at 450°, 550° and 650°C are shown in Figure 6. The TEM images of the samples confirm the nanometric size of the particles in the range of 5–90 nm. The histograms show that the mean particle size of the no-calcined and calcined samples at 450°, 550° and 650°C are about 28, 33, 36 and 41 nm, respectively. It is clear from TEM images that the nanoparticles grew as the calcination temperature increased [9].

TEM images results like XRD (Scherer's formula) results confirm the nanometric sizes of the samples, but TEM shows the mean size of the particles more than XRD. This difference in the size refers to this fact that "TEM shows the size of the particles and XRD shows the size of the crystallites". In addition, the Scherer's formula (2) has good results for single crystals (our samples are not single crystals) and we use Scherer's formula (2) only to confirm the nanometric size of the samples before using TEM images [8].

TEM Electron Diffraction or Selected Area Electron Diffraction (SAED) pattern of no-calcined Dy<sub>2</sub>O<sub>3</sub> nano-

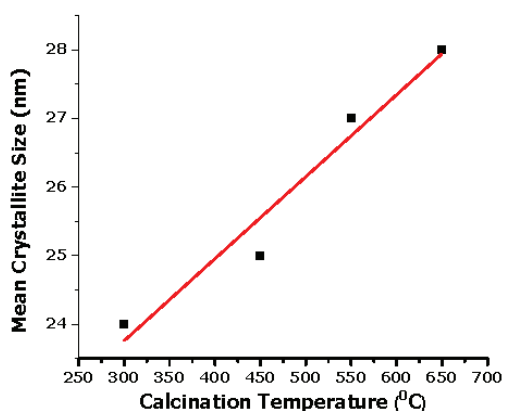


**Figure 5.** Variation of mean crystallite size against calcination temperature. The first point is for no-calcined sample and the temperature is the furnace temperature.

particles is shown in Figure 7. Since for other samples there is not any significant variation in SAED pattern, just SAED pattern of no-calcined sample is shown in this research. It is obvious from the ordered points that the crystal structure is formed and this pattern is for a single crystal. This pattern is related to one of the standard indexed diffraction patterns for bcc crystals in  $[-111]$ . The electron beam was perpendicular to the Dy<sub>2</sub>O<sub>3</sub> (111) plane. Some spots are marked with  $(hkl)$  indices [10–12].

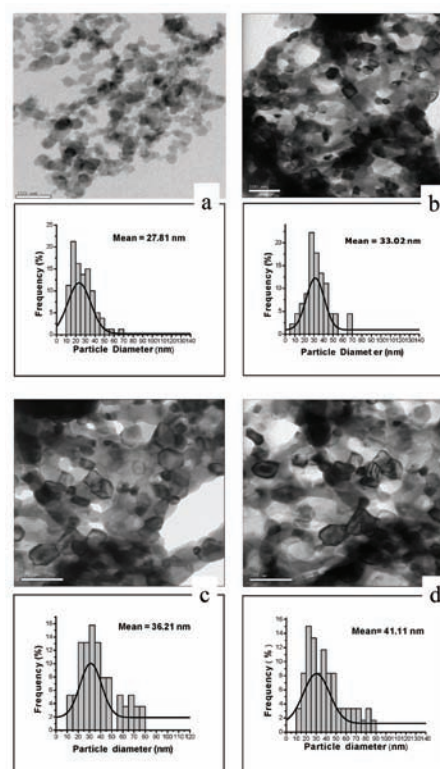


**Figure 6.** TEM images of Dy<sub>2</sub>O<sub>3</sub> prepared a) without calcination temperature, b) at 450°C calcination temperature, c) at 550°C calcination temperature, d) at 650°C calcination temperature.

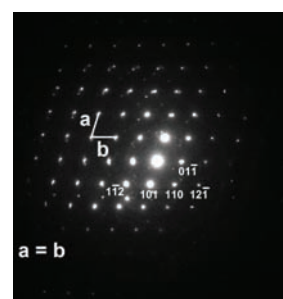


**Figure 7.** TEM diffraction pattern of no-calcined Dy<sub>2</sub>O<sub>3</sub> nanoparticles.

### 3.3 Photoluminescence Studies

The photoluminescence spectrum of no-calcined  $\text{Dy}_2\text{O}_3$  sample and other samples calcined at three different calcination temperatures, excited with 355 nm laser, are shown in Figure 9. As the pattern obtained from calcined samples at 550°C (Figure 9c) and 650°C (Figure 9d) depict, 4 strong peaks are overt at about 451, 485, 582 and 680 nm. For no-calcined sample (Figure 9a) and calcined sample (Figure 9b) it shows just 3 peaks at about 445, 480 and 580 nm which for no calcined sample peak 3 (580 nm) is very weak. For sample one (9a) or no calcined sample, the first peak at comparing with other ones show supreme intensity and height.

Obviously, from Figure 9, as the calcination temperature rose from 450°C to 650°C, the first peak exhausts while the second one gains the momentum, the phenomenon reach its clear stage at 650°C. Moreover for sample 3 and 4 (Figures 9c and 9d) there are three important PL emission peaks at about 485, 582 and 680 nm.

Figure 8, shows energy diagram of Dy ion with characteristic transitions present in the emission spectra. So, in Figure 9, 3 peaks located at about 485, 582 and 680 nm has been previously attributed to  ${}^4\text{F}_{9/2} \rightarrow {}^6\text{H}_{15/2}$  (blue),  ${}^4\text{F}_{9/2} \rightarrow {}^6\text{H}_{13/2}$  (yellow) and  ${}^4\text{F}_{9/2} \rightarrow {}^6\text{H}_{11/2}$  (red) transitions of  $\text{Dy}^{3+}$  ions [13]. One can justify one remaining peaks at about 450 nm using the feasible thermal treatment effect. Sample 1 (Figure 9a) has been prepared by a combustion reaction in 300°C without any further calcination while the rest of samples were calcined at higher temperature after reaction accomplishment. Seemingly, initial reaction of glycine in presence of oxygen has produced number of by-products with photoluminescence ability. Higher temperatures annihilate these compounds; as a result, the first peak diminishes while the other peaks have intensified. Increase of the calcination temperature leads to intensify of the peaks, which refers to crystal growth and more oxygen vacancy distribution. So applying calcination temperature improved optical properties of the samples. Based on the available evidence it has believed that in higher calcination temperatures like 1000°C only 3 peaks (at about 485, 582 and 680 nm) will remain in light of utter decomposition of by-products reactions and ultimate crystal formation.

Photoluminescence spectroscopy can be used as a mean for band gap measurement. Farsi and et al has successfully employed this approach for band gap measurement of  $\text{NiWO}_4$  sample [14]. According to Figure 8, among 3 different transitions the one occurred in about

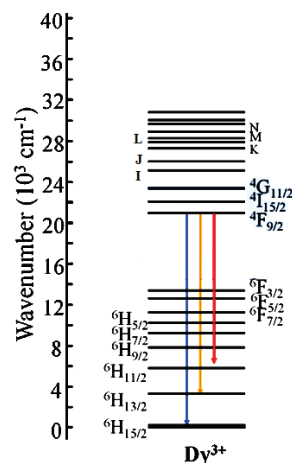


**Figure 8.** Energy diagram of Dy ion with characteristic transitions present in the emission spectra.

Source: Borja-Urbya et al. [13]

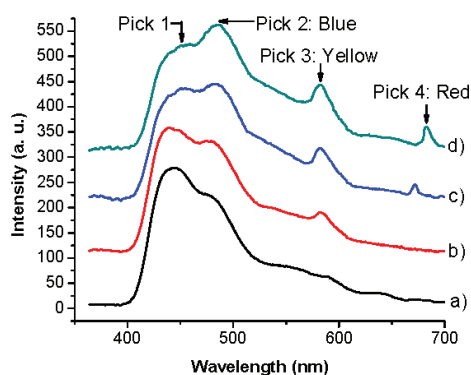


**Figure 9.** Emission spectra ( $\lambda_{\text{exc}} = 267 \text{ nm}$ ) of  $\text{Dy}_2\text{O}_3$  samples a) sample 1, no-calcined sample, b) sample 2, calcined sample at 450°C, c) sample 3, calcined sample at 550°C, d) sample 4 calcined sample at 650°C.

480 nm has been ascribed to direct transition of  $\text{Dy}_2\text{O}_3$  sample which is equal to 2.625 eV.

## 4. Conclusion

A novel approach for the synthesis of the  $\text{Dy}_2\text{O}_3$  nanoparticles has been developed without applying calcination temperature. XRD results show that all samples consist of no-calcined sample obtained directly from combustion method and calcined samples at 450°, 550° and 650°C exhibited cubic structure. The crystallite size was estimated by XRD, using Scherrer's formula (2), 24, 25, 27 and 28 nm for no-calcined sample and samples calcined at 450°, 550° and 650°C, respectively. TEM and XRD results indicated that increasing the calcination

temperature improved the crystallinity. TEM images show that the average diameter of no-calcined sample and samples calcined at 450°, 550° and 650°C are 28, 33, 36 and 41 nm, respectively. TEM Electron Diffraction (SAED) pattern of Dy<sub>2</sub>O<sub>3</sub> nanoparticles shows one of the standard indexed diffraction patterns for bcc crystals in  $[-111]$ . PL results confirmed that the samples possess strong emission in the visible region. Samples calcined at 550° and 650°C clearly show three peaks, related to Dy<sup>3+</sup> transitions in emission spectra. For the PL, increase of the calcination temperature leads to intensify of the peaks, which refers to crystal growth and more oxygen vacancy distribution. Band gap was measured by PL results about 2.625 eV.

## 5. References

1. Boddu S (2011). Synthesis and characterization of lanthanide ions doped nanomaterials, Bhabha Atomic research centre, Ph D thesis.
2. Happy, Tok A I Y et al. (2007). Homogeneous precipitation of Dy<sub>2</sub>O<sub>3</sub> nanoparticles—effects of synthesis parameters, *Journal of Nanoscience and Nanotechnology*, vol 7(3), 907–915.
3. Sato S, Takahashi R et al. (2009). Basic properties of rare earth oxides, *Applied Catalysis A: General*, vol 356(1), 57–63.
4. Collusi S, Leitenburg C D et al. (2004). The role of rare earth oxides as promoters and stabilizers in combustion catalysts, *Journal of Alloys and Compounds*, vol 374(1–2), 387–392.
5. Kishi H, Mizuno Y et al. (2003). Base-metal electrode-multilayer ceramic capacitors: past, present and future perspectives, *Japanese Journal of Applied Physics*, vol 42(1), 1–15.
6. The U. S. Department of Energy (2010). Available from: <http://ow.ly/3pPdV>
7. Klug P, and Alexander L E (1954). X-Ray diffraction procedures for polycrystalline and amorphous materials, 1st Edn., Chapter 9, Wiley, New York, 903–700.
8. Zelati A, Amirabadizadeh A et al. (2011). Preparation and characterization of barium carbonate nanoparticles, *International Journal of Chemical Engineering and Applications*, vol 2(4), 306–310.
9. Zak A K, Majid A W H et al. (2011). Synthesis and characterization of ZnO nanoparticles prepared in gelatin media, *Material Letters*, vol 65(1), 70–73.
10. Srivastava A K, Kishore R et al. (2004). Electron microscopy and diffraction analysis of nano-structured prussian blue thin films, *Indian Journal of Engineering & Material Sciences*, vol 11(4), 315–318.
11. Romeu D, Gomez A et al. (2011). Electron diffraction and HRTEM structure analysis of nanowires, *Nanowires - fundamental Research*, 1st Edn., Chapter 20, Hashim A (Ed.), InTech, Croatia, 461–484. Available from: [www.intechopen.com/books/nanowires-fundamental-research/electron-diffraction-and-hrtem-structure-analysis-of-nanowires](http://www.intechopen.com/books/nanowires-fundamental-research/electron-diffraction-and-hrtem-structure-analysis-of-nanowires)
12. Basic Crystallography and Electron Diffraction from Crystals, CHEM 793, 2008 Fall, Lecture 14, Available from: [nstg.nevada.edu/tem/chem793-2011/Lecture\\_14\\_1\\_CHEM793.pdf](http://nstg.nevada.edu/tem/chem793-2011/Lecture_14_1_CHEM793.pdf)
13. Borja-Urbya R, Diaz-Torres L A et al. (2011). Strong broad green UV-excited photoluminescence in rare earth (RE=Ce, Eu, Dy, Er, Yb) doped barium zirconate, *Materials Science and Engineering B*, vol 176(17), 1388–1392.
14. Farsi H, and Hosseini S A (2013). The electrochemical behaviors of methylene blue on the surface of nano-structured NiWO<sub>4</sub> prepared by coprecipitation method, *Journal of Solid State Electrochemistry*, vol 17(7), 2079–2086.